Journal of Alloys and Compounds 877 (2021) 160189

Contents lists available at ScienceDirect

Journal of Alloys and Compounds

journal homepage: www.elsevier.com/locate/jalcom

Synthesis and gas sensing properties of NiO/ZnO heterostructured nanowires

Sikai Zhao[a,c,d], Yanbai Shen[a,b,*], Yong Xia[c,d], Aifei Pan[c,d], Zhou Li[c,d], Carlo Carraro[c,d], Roya Maboudian[c,d,*]

[a] School of Resources and Civil Engineering, Northeastern University, Shenyang 110819, China
[b] State Key Laboratory of Rolling and Automation, Northeastern University, Shenyang 110189, China
[c] Department of Chemical and Biomolecular Engineering, University of California, Berkeley, CA 94720, USA
[d] Berkeley Sensor & Actuator Center, University of California, Berkeley, CA 94720, USA

ARTICLE INFO

Article history:
Received 19 February 2021
Received in revised form 18 April 2021
Accepted 25 April 2021
Available online 5 May 2021

Keywords:
Heterostructure
NiO
ZnO
Nanowires
Ethanol sensing
Gas sensing

ABSTRACT

In this study, we report on the synthesis of the NiO/ZnO heterostructured nanowires by a facile two-step liquid phase route and their gas sensing characteristics employing Au interdigitated electrodes integrated on a miniature ceramic heater. Microstructural characterizations indicate that flocculent NiO particles are uniformly assembled on the outer surfaces of the single-crystalline ZnO nanowires, with diameters around 50 nm and lengths ranging from 500 nm to several μm. The gas sensing investigation indicates that the sensors based on NiO/ZnO heterostructured nanowires exhibit high sensitivity towards ethanol, good reversibility, reproducibility, stability, robustness towards humidity, and fast response/recovery rates at the determined optimum operating temperature of 300 °C. Interestingly, the sensor shows higher ethanol response but longer recovery time in N_2 compared with those in air. An ethanol sensing mechanism is proposed to explain the experimental results.

1. Introduction

Gas sensors, the devices that transfer information about the presence and concentration of gases of interest into detectable electrical signals, play an important role in many industries, environmental protection, health and safety, and medical systems, among others [1,2]. The sensing signal transformation can be achieved by using different principles resulting in various types of gas sensors [3,4]. Conductometric semiconducting gas sensors are designed based on the resistance change of a semiconducting material caused by the interfacial reaction between the gas and the surface of the sensing material, and have captured a large portion of the gas sensing market due to their solid state, low cost, high reliability, and easy operation [5,6]. While they have been employed for the detection of various gases and in many applications, several issues remain including their limited selectivity and humidity interference. As a core part of a semiconducting gas sensor, sensing materials play a key role in determining the sensing performance of the device, with the microstructure and surface properties being the dominant factors.

ZnO, a II-IV metal oxide semiconductor (MOS) with a band gap of 3.37 eV at room temperature, is an important multifunctional material with a broad range of technological applications, especially for optical and electronic related devices [7,8]. ZnO is also considered one of the most promising materials for gas sensing and has received extensive attention due to its high chemical and thermal stability, low cost, and tunable chemical and electronic properties [9,10]. Stimulated by the unique properties and great application potential, various ZnO nanostructures, such as nanorods, nanosheets, and nanoflowers have been explored and reported [11–13]. Amid these structures, one-dimensional ZnO materials have attracted increasing interest because of their high specific surface area, comparable dimensions to the surface charge region, high crystallinity, ease of surface functionalization, and good electron transport capacity [14,15]. Thus, one-dimensional ZnO nanowires are expected to overcome the present limitations of MOS gas sensors [16,17].

To better meet the requirements of different working conditions, surface functionalization of pristine MOS materials is usually required to further regulate or improve their gas sensing properties.

* Corresponding author at: School of Resources and Civil Engineering, Northeastern University, Shenyang 110819, China.
** Corresponding author at: Department of Chemical and Biomolecular Engineering, University of California, Berkeley, CA 94720, USA.
E-mail addresses: shenyanbai@mail.neu.edu.cn (Y. Shen), maboudia@berkeley.edu (R. Maboudian).

https://doi.org/10.1016/j.jallcom.2021.160189
0925-8388/

One of the most attractive strategies is constructing MOS-MOS heterostructures to take full advantage of the two different types of sensing materials [18]. The difference in the work functions between the two materials results in a charge depletion or accumulation region at the heterojunction [19], providing a great possibility to tailor the sensing characteristics of the MOS sensing materials [20]. Another advantage of MOS-MOS heterostructures in gas sensing is their synergistic effects. For some multi-step gas sensing reactions, the tested gas may prefer to react with one of the two materials and the resulting products may react with the other material most readily to bring the reactions to completion [21,22]. Furthermore, improvements in the selectivity and reduction in humidity interference of the host sensing materials by constructing heterostructures have been recently reported [23].

In this work, one-dimensional NiO/ZnO heterostructured nanowires are synthesized by depositing flocculent NiO particles on the surface of the ZnO nanowires. The gas sensing properties of the prepared samples are investigated using a miniature ceramic-based heater. The sensor shows good ethanol sensing performance over a wide range of relative humidity (RH) at the selected optimum operating temperature of 300 °C. Furthermore, the sensor exhibits a much higher ethanol response in the background gas of N_2 than in air. A possible sensing mechanism is discussed based on the experimental results and reported literature.

2. Experimental

2.1. Preparation of NiO/ZnO heterostructured nanowires

NiO/ZnO heterostructured nanowires were prepared by constructing NiO on the surface of ZnO nanowires. ZnO nanowires were firstly synthesized by a solvothermal method following our previously reported recipe [24]. Briefly, zinc acetate dihydrate (0.44 g) was used as the source of Zn, absolute ethanol (117 mL) was used as the solvent, sodium hydroxide (2.5 g) was used to adjust the pH of the precursor, sodium dodecyl sulfate (0.1 g) and polyethylene glycol 400 (27 mL) were used as surfactants to control the structure of the product. All of the above reagents were added into a plastic beaker and then magnetically stirred for 1 h to completely dissolve and mix. The resultant transparent solution was then transferred into a Teflon bottle, which was subsequently sealed into a stainless autoclave for the followed reaction. The solvothermal reaction was conducted at 140 °C and maintained for 16 h. After the reaction, the products were rinsed with water and ethanol, and then dried at 60 °C in a vacuum oven.

To grow NiO on the surface of the ZnO nanowires and construct the heterostructure, a solution-based precipitation route was designed. The prepared ZnO nanowires (0.0972 g) were dispersed in 30 mL deionized water with the assistant of ultrasonication and magnetic stirring. Then, 1.2 mL of 0.1 M nickel nitrate solution was added to the dispersion solution while stirring. After 10 min, 5 mL mixed solution of potassium persulfate solution (4.5 mL, 0.2 M) and ammonia solution (0.5 mL, 25%–28%) was dropwise added to the above solution for another 1 h stirring. The samples were centrifuged and then washed using water and ethanol, dried at 60 °C, and finally annealed at 500 °C for 3 h to improve the crystallinity and stabilize the structure.

2.2. Characterizations of the prepared samples

The crystallinity and phase structure of the prepared materials were characterized by X-ray diffraction spectroscopy (XRD, PANAlytical X′Pert Pro) using Cu Kα radiation at wavelength of 1.5406 Å. The operation voltage and current were respectively set to be 40 kV and 40 mA, respectively, and the diffraction data in the 2θ range of 20–80° were recorded. The structure and morphology of the materials were investigated by field emission scanning electron microscopy (FESEM, ZEISS Ultra Plus) at the operating voltage of 15 kV, and transmission electron microscopy (TEM, JEM-2100 F) at the operating voltage of 200 kV. During the FESEM and TEM analyses, the energy-dispersive X-ray spectroscopy (EDS) and elemental mapping images were also recorded for the confirmation of the elemental composition and distribution of the products, respectively. The detailed near-surface chemical composition was probed by X-ray photoelectron spectroscopy (XPS, Thermo Scientific Escalab 250Xi) using monochromatic Al K_α source.

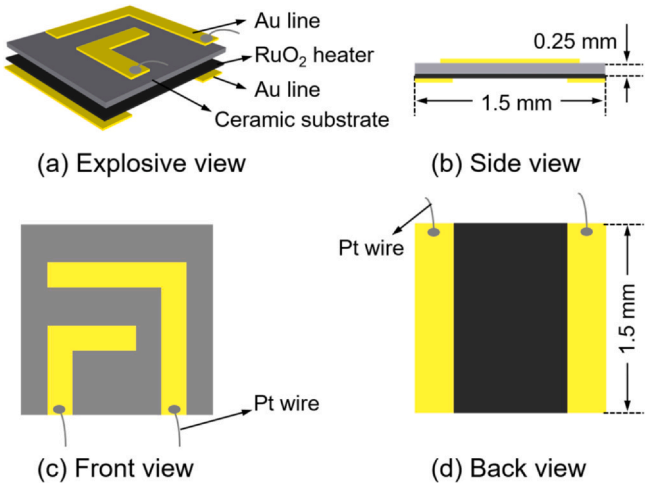

Fig. 1. Structure of the gas sensor with the integrated heater.

2.3. Gas sensor fabrication and gas sensing tests

Fig. 1 shows the structure of the gas sensing electrode (Sino Aggtech), that is used to evaluate the gas sensing properties of the prepared materials in this study. As can be seen in this figure, a square 1.5 × 1.5 mm^2 ceramic plate with a thickness of 0.25 mm was employed as the substrate. On the front side of the ceramic plate, interdigitated Au thin lines were printed as the sensing electrodes, while a RuO_2 heating layer and two parallel Au thin lines were printed on the backside to control the operating temperature of the sensor. The as-synthesized NiO/ZnO nanowires were homogeneously suspended in ethanol with the assistant of ultrasonication, which was then drop-casted on the front side of the ceramic plate followed by a 24 h aging at the operating temperature of 350 °C.

The gas sensing manifold was detailed in our previous reports [25,26]. The fabricated sensor was wire-bonded to a 4-pin socket and then placed into the test chamber within a volume of ~1 cm^3. The tested gases including ethanol (Airgas, 978 ppm in N_2), formaldehyde (Praxair, 22.1 ppm in N_2), acetone (Airgas, 409 ppm in N_2), CO_2 (Airgas, 20,200 ppm in N_2), NH_3 (Praxair, 9.39 ppm in N_2), and NO_2 (Praxair, 21.8 ppm in N_2) were individually diluted with predried house air and then flowed to the test chamber with a total flow rate of 300 sccm. All the mass flow controllers (Bronkhorst) in the gas delivery system were controlled by a LabView-based computer program. A Keithley 2602 source-meter was used to monitor the sensor resistance and control the heater temperature. A bias voltage of 1 V was applied to the sensing materials and the applied voltage on the heater was changed to provide different operating temperatures. An open Java-based software suit, Zephyr, is employed to collect and record the data from the source meter and gas delivery system.

The sensor response was defined as R_a/R_g, where R_a and R_g were the sensor resistance upon exposure to fresh air and target gas,

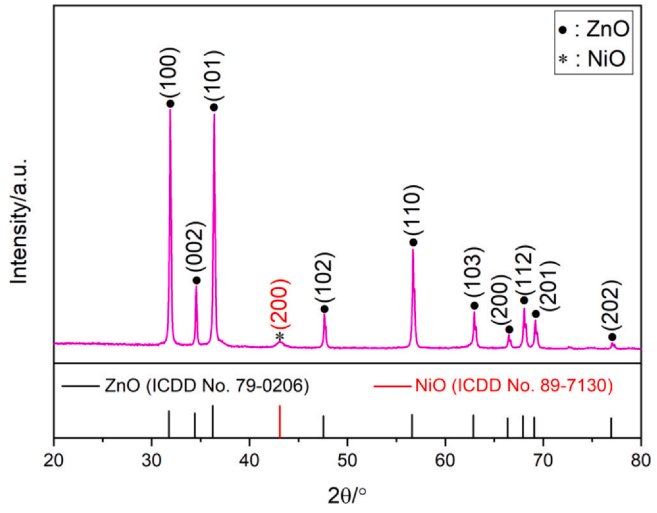

Fig. 2. XRD pattern of the NiO/ZnO heterostructured nanowires.

respectively. The response and recovery times were defined as the times for the sensor to achieve 90% of the full resistance upon exposure to the target gas and its removal, respectively.

3. Results and discussion

3.1. Characterizations

Fig. 2 shows the XRD pattern of the prepared NiO/ZnO nanowires, indicating both ZnO and NiO phases. The peaks at 31.8°, 34.4°, 36.3°, 47.5°, 56.6°, 62.9°, 66.4°, 67.9°, 69.1°, and 77.0° are indexed to hexagonal wurtzite structured ZnO according to the ICDD card No. 79-0206, while the peak at around 43.1° matches well with ICDD card No. 89–7130 of cubic NiO. The results indicate that the NiO/ZnO composite is successfully synthesized. In addition, no other peaks related to any impurities are detected in the pattern, demonstrating the prepared sample is of high phase purity.

Fig. 3 shows the FESEM images with different magnifications and the corresponding EDS pattern of the prepared NiO/ZnO heterostructured nanowires. As can be seen in the low-magnification images of Fig. 3(a, b), the prepared products consist of uniform nanowires up to several micrometers in length. The nanowires are interlaced with each other forming a porous network, which can provide effective paths for gas diffusion during the gas sensing process and improve the gas sensing performance [27,28]. Fig. 3(c) displays the FESEM image under high magnification, indicating that the nanowires have a uniform diameter in the range of 30–50 nm. More importantly, compared with the FESEM images of pristine ZnO nanowires in Fig. S1, the second phase additives can be clearly observed on the surface of the ZnO nanowires of the composite materials. The corresponding EDS spectrum is exhibited in Fig. 3(d), highlighting that no peak related to other elements besides Zn, Ni, and O can be observed in the spectrum, further confirming the high purity of the prepared NiO/ZnO composite nanowires. Furthermore, the detected atomic ratio of Ni to Zn is 8.2%, which is somewhat lower than that (10%) based on the starting solution. This may be caused by the loss of Ni during the reaction and washing process.

More insight into the microstructure of the prepared NiO/ZnO heterostructured nanowires was obtained by TEM. As shown in Fig. 4(a), the nanowire possesses a rough surface with a relatively uniform diameter, which agrees well with the FESEM characterization results. Additionally, the one-dimensional heterostructure can be clearly observed, where loose flocculent NiO particles are assembled on the surfaces of ZnO nanowires. Fig. 4(b) shows the HRTEM image of the NiO/ZnO, in which the different lattice fringes can be clearly observed. The well-defined interplanar spacing of 2.60 Å in ZnO core region corresponds to the (002) crystal planes of wurtzite structured ZnO [29], and the lattice fringes with *d*-spacings of 2.08 and 2.40 Å in NiO shell region are assigned to the (200) and (111) crystal planes of cubic NiO [30,31], respectively. Fig. 4(b) inset provides the corresponding SAED pattern. The clear spot array and some diffraction rings can be observed in this pattern, indicating the coexistence of monocrystalline ZnO and polycrystalline NiO. The elemental mapping images of a single NiO/ZnO nanowire shown in Fig. 4(d, e, f) indicate that a uniform wire-like distribution of Zn, Ni, and O elements is obtained. Then, the color dot of Zn element in

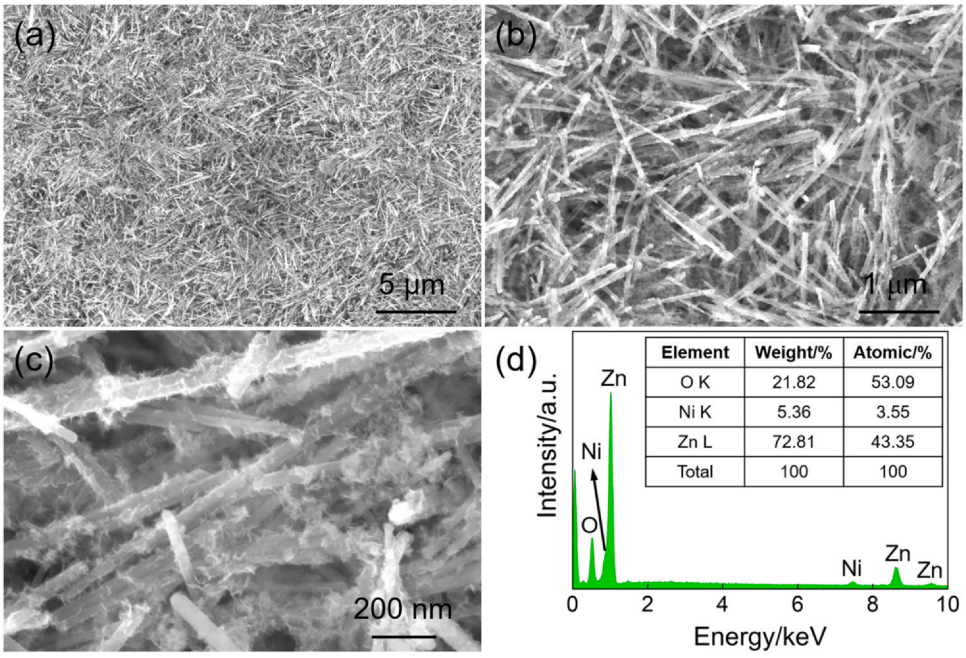

Fig. 3. (a–c) FESEM images of NiO/ZnO heterostructured nanowires with different magnifications, (d) the corresponding EDS pattern.

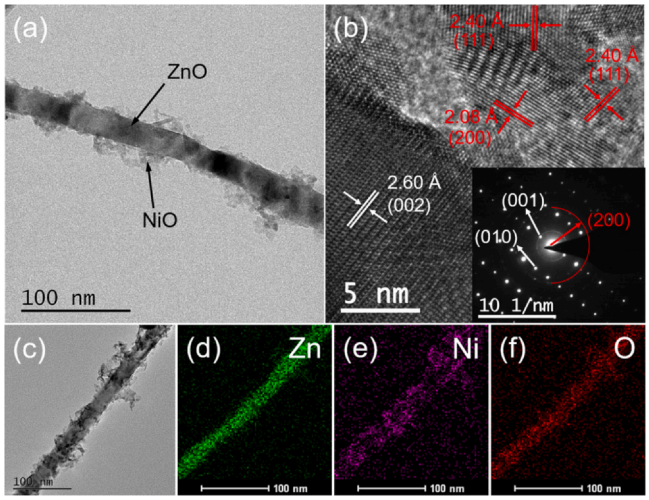

Fig. 4. TEM characterization results of NiO/ZnO heterostructured nanowires: (a) typical TEM image; (b) HRTEM image and the corresponding SAED pattern (insert); (c-f) a typical TEM image of a single nanowire and the corresponding elemental mapping images for Zn, Ni, and O, respectively.

Fig. 4(d) is denser than that of Ni element in Fig. 4(e), demonstrating that the content of Zn element in the materials is higher than that of Ni element, which is consistent with the pre-defined Ni/Zn atomic ratio of ~10% in raw materials. In addition, it can be found that the distribution region of Ni and O elements are slightly broader than that of Zn element along the nanowire. This is consistent with the FESEM images that suggests NiO distributes on the outer surfaces of ZnO nanowire, providing further evidence for the formation of NiO/ZnO heterostructure.

The XPS characterizations were performed to further determine the surface composition and chemical sate of the synthesized NiO/ZnO heterostructured nanowires. All the peaks were calibrated using the binding energy of C 1 s at 248.8 eV as a reference. The full scan spectrum in Fig. 5(a) confirms that the prepared sample is composed of Zn, Ni, and O elements with high purity. Fig. 5(b) shows the Zn 2p region of the spectrum, with the peaks at the binding energies of 1021.86 and 1044.77 eV assigned to Zn $2p_{3/2}$ and Zn $2p_{1/2}$, respectively [32]. The energy splitting value of 22.91 eV and the energy loss feature between these two peaks demonstrate the chemical state of Zn^{2+} in NiO/ZnO nanowires [33]. The high-resolution XPS spectrum of Ni 2p is given in Fig. 5(c). The peaks located at the binding energies of around 855 and 873 eV are attributed to Ni $2p_{3/2}$ and Ni $2p_{1/2}$, respectively, where the significant multiple-split feature can also be observed [34]. The other two peaks at around 861 and 879 eV are assigned to the satellite peaks of Ni $2p_{3/2}$ and Ni $2p_{1/2}$, respectively [35]. The results confirm the existence of Ni^{2+} in the synthesized sample. The O 1 s spectrum, which comes from both the ZnO core and NiO shell of NiO/ZnO nanowires, is shown in Fig. 5(d) and is deconvoluted into two components. Based on the previous reports, the peak centered at 530.94 eV is attributed to the Zn—O and Ni—O bonds in the crystal lattice of NiO/ZnO nanowires [36], while the peak at around 532.24 eV is regarded as the signal of surface adsorbed oxygen species (such as – OH, O^{2-}, and O^{-}) and oxygen deficient [37,38].

3.2. Gas sensing properties

The ethanol sensing behavior of NiO/ZnO based sensor at different operating temperatures was firstly studied to determine the optimum operating temperature. Fig. 6(a) shows the responses of the sensor to 20 ppm ethanol at different operating temperatures. The response increases sharply with increasing the operating temperature from 100 °C to 300 °C and reach a maximum response of ~49 at 200 °C. Then, the response declines with further increase in temperature. When the sensor is exposed to ethanol, the change of the sensor resistance (sensor sensing signal) is known to be related to the redox reaction between ethanol molecules and chemisorbed oxygen species on the surface of the sensing materials. When the operating temperature is relatively low, there is not sufficient energy for this reaction, and thus, a low response and long response/recovery times [38]. On the other hand, at relatively high operating temperatures, the gas molecules desorb from the surface of the sensing materials before reaction, leading to a decrease in the sensor response as seen in Fig. 6(a). Fig. 6(b) displays the response and recovery times to 20 ppm ethanol at different operating temperatures. The response and recovery times shorten quickly when raising the operating temperature. The sensor does not reach full recovery at heater temperatures of 150 °C and below after exposure to ethanol (Fig. S2(a, b)). Although the sensor shows the highest response at 200 °C, the response/recovery time is rather long. Taking both response and response/recovery rates into consideration, in this study, heater temperature of 300 °C is selected as the optimum operating temperature for ethanol sensing. At this temperature, the response and recovery times are ~4 and 28 s for 20 ppm ethanol, respectively. Furthermore, the sensing performance of pristine ZnO nanowires based sensor to 20 ppm ethanol at 300 °C was also investigated in Fig. S3. The corresponding response is 4.7, while the response and recovery times are 4 s and 110 s, respectively. Clearly, NiO/ZnO composite materials are more sensitive to ethanol, with a much faster recovery speed.

Fig. 7(a) displays the dynamic response and recovery curves of the sensor, held at 300 °C, to repetitive sensing cycles with ethanol concentration ranging from 3 to 100 ppm. The sensor shows fast response and recovery rates with an excellent reversibility and a stable baseline resistance. The sensor resistance drops quickly and then reaches steady state upon exposure to ethanol. After the ethanol is purged out, the sensor resistance recovers in a short time. Such resistance change characteristic is consistence with the typical sensing behavior of n-type metal oxide semiconducting gas sensing materials to reducing gases, suggesting that the NiO/ZnO heterostructured nanowires maintain the n-type semiconducting characteristic. The responses of the sensor to different ethanol concentrations at 300 °C were calculated and presented in Fig. 7(b). It can be seen that the sensor response shows a monotonic increase with increased ethanol concentration ranging from 3 to 100 ppm. Furthermore, an effective response of 2.3 can be detected for a low ethanol concentration of 3 ppm. Such a detectable concentration is much lower than the limit of the human sense of smell (~6.1 ppm) [39].

The cross-sensitivity was then checked by measuring the sensor responses to several interfering gases including carbon dioxide, ammonia, formaldehyde, nitrogen dioxide, and acetone at the operating temperature of 300 °C. As can be seen in Fig. 8, the sensor responses to carbon dioxide (1000 ppm), ammonia (8 ppm), formaldehyde (15 ppm), nitrogen dioxide (20 ppm), and acetone (20 ppm) are 1.2, 1.8, 2, 1 and 1.2, which are much lower than the sensor response to ethanol (20 ppm), suggesting that the sensor is much more sensitive to ethanol than these interfering gases. The observed sensing characteristics can be related to the nature of ZnO and NiO, the selected operating temperature, and the chemical properties of ethanol, as discussed in our previous report [40].

Fig. 9(a) shows the dynamic response and recovery curves of the sensor upon alternative exposure to air and 20 ppm ethanol. The excellent reversible and reproducible real-time response can be clearly observed with the sensor exhibiting a consistent response and recovery behavior in every sensing cycle. To further evaluate the stability of the sensor, the responses of the sensor to various concentrations of ethanol were also tested and recorded on the 15th (Fig. 9(b)) and 30th days (Fig. 9(c)). Compared with the sensing data

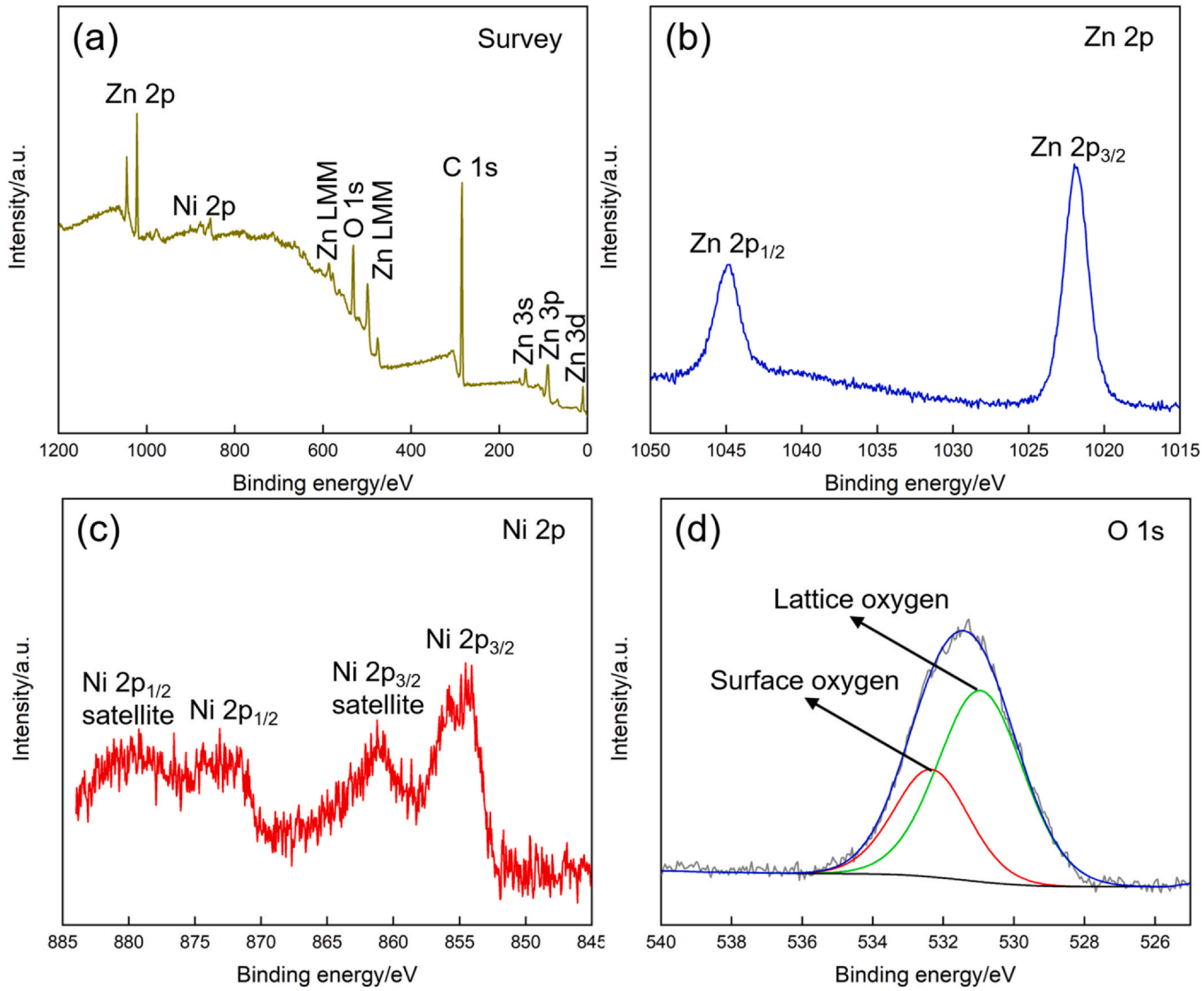

Fig. 5. XPS spectra of NiO/ZnO heterostructured nanowires. (a) Survey scan spectrum; (b) Zn 2p; (c) Ni 2p; (d) O 1 s regions.

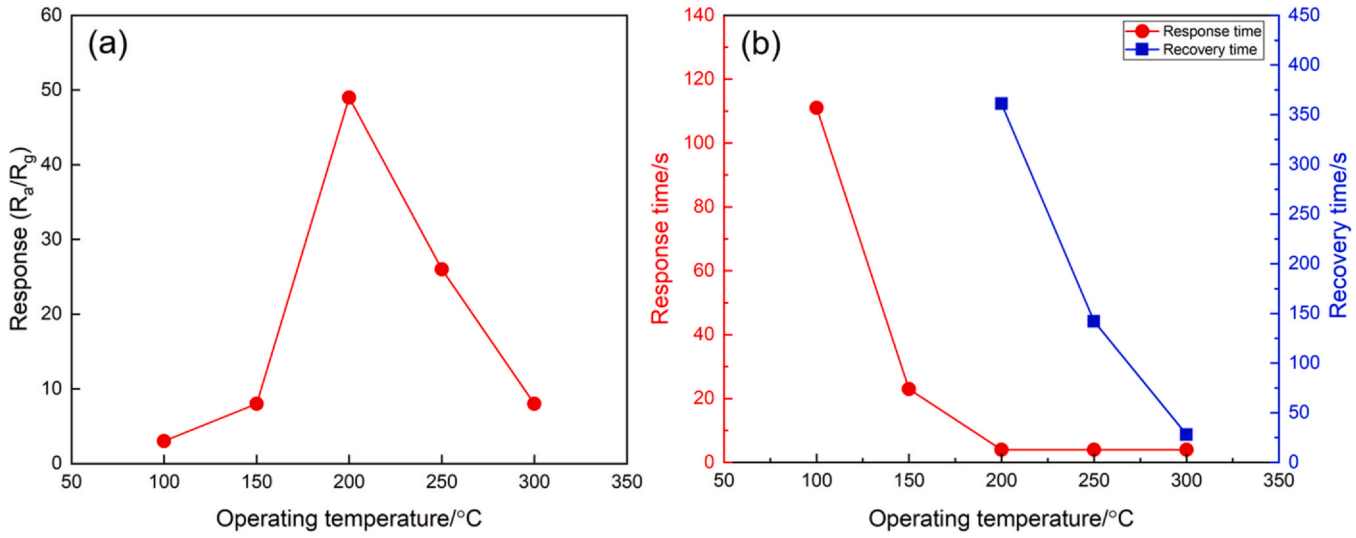

Fig. 6. (a) Responses and (b) response/recovery times of NiO/ZnO heterostructured nanowires upon exposure to 20 ppm ethanol at different operating temperatures.

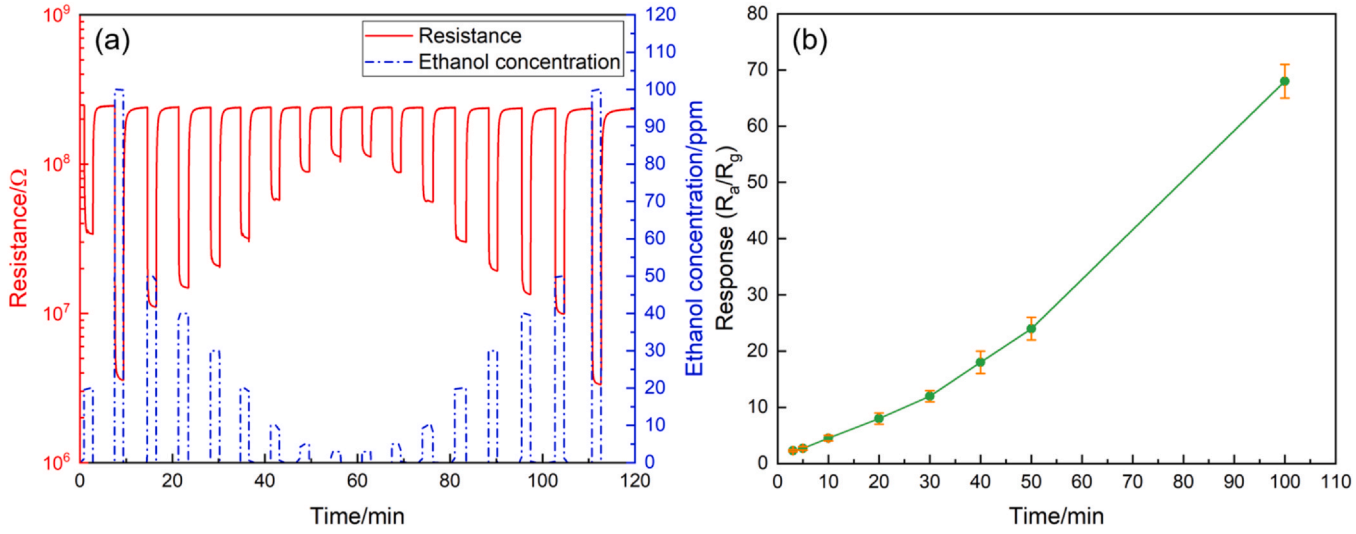

Fig. 7. (a) Transient resistance and (b) responses of NiO/ZnO heterostructured nanowires upon exposure to different concentrations of ethanol at 300 °C.

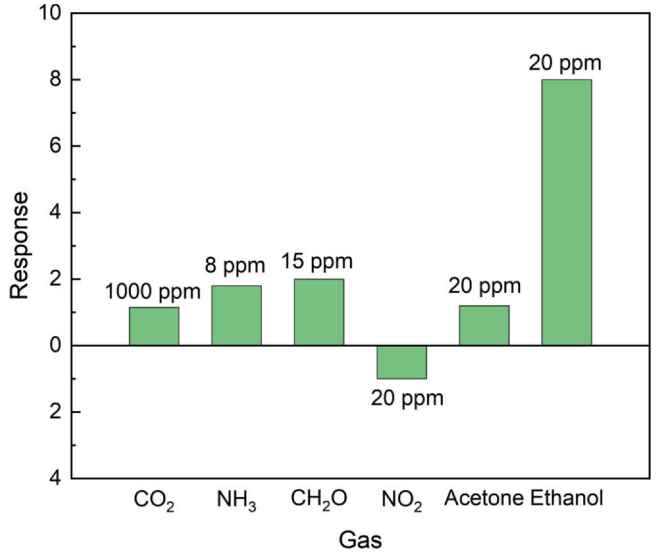

Fig. 8. Responses of NiO/ZnO heterostructured nanowires to various gasses at the operating temperature of 300 °C.

collected on the 1st day, the sensor response showed no obvious deviation to the same concentration of ethanol. Meanwhile, only a small drift of the baseline resistance of the sensor is observed after 30 days. The results demonstrate the good long-term stability of the sensor for ethanol sensing.

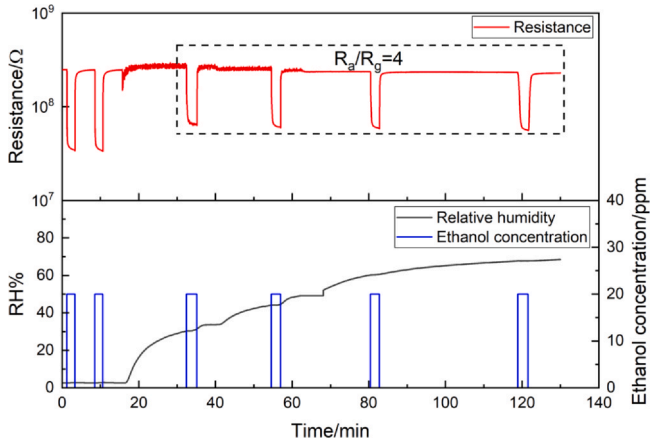

Fig. 10. (top) Dynamic response and recovery curves of NiO/ZnO heterostructured nanowires to (bottom) 20 ppm ethanol at different humidity conditions.

Relative humidity is usually reported to have a significant effect on the gas sensing performance of MOS sensors. Hence, the sensing performance of the NiO/ZnO based sensor at different humidity conditions was studied. As can be seen in Fig. 10, the responses of the first two sensing cycles in dry air (~3% RH) is 7, which is consistent with the sensing results in Figs. 7 and 9, indicating the good reproducibility of the sensor. In addition, it is found that the baseline resistance of the sensor shows higher noise level when the humidity is increased, which can be mainly ascribed to the fluctuation of the

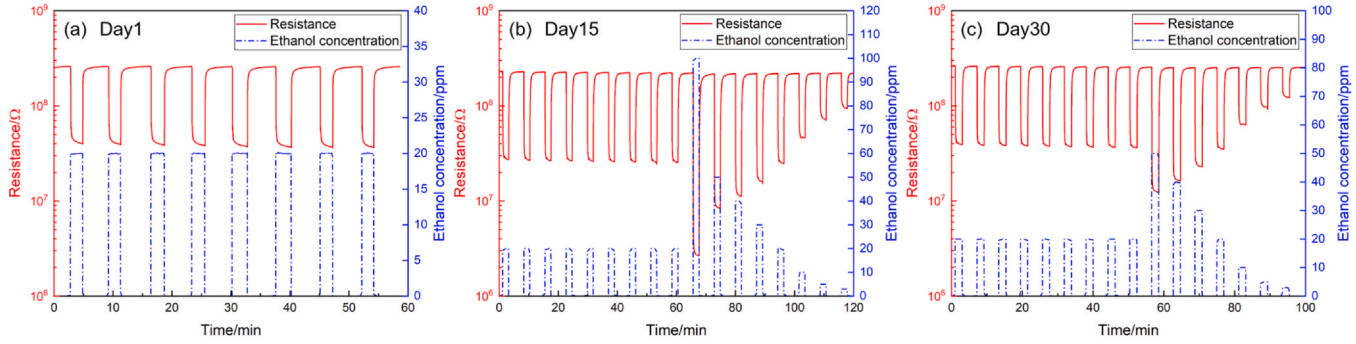

Fig. 9. Dynamic response and recovery curves of the NiO/ZnO heterostructured nanowires to various concentrations of ethanol. (a), (b), and (c) are the data collected on the 1st, 15th, 30th day, respectively.

gas flow in the gas delivery system when increasing the humidity, especially under low humidity conditions. It may also be related to the dynamics of surface adsorption/desorption processes when transferring the sensor from a dry condition to a wet one. The sensor response decreases to 4 when the RH increases to around 30% due to the competitive adsorption of water and ethanol [41]. But the sensor maintains a constant response value of 4 as the RH increases to 70%. Meanwhile, it can be observed that the sensor still exhibits fast response and recovery rates even at relative humidity of 70%. Notably, the sensor keeps a relatively stable baseline resistance without any obvious decrease over the entire tested RH range of 3%– 70%. For comparison, the sensing performance of the pristine ZnO based sensor at different humidity conditions was shown in Fig. S4. It can be seen that the sensor resistance decreases sharply once the relative humidity increases, and the sensor response to 20 ppm ethanol decreases from 4.7 to 2.5 when the relative humidity increases from ~4% to ~50%. The results suggest that NiO layer can reduce the effect of relative humidity to some extent [23], especially for the sensor baseline resistance stabilization.

3.3. Gas sensing mechanism discussion

ZnO and NiO are typically n- and p-type semiconducting materials, respectively. From Figs. 7 and 9, it can be deduced that the NiO/ZnO heterostructured nanowires show the n-type behavior, indicating that the sensing process of the NiO/ZnO composite materials is dominated by the n-type ZnO nanowires. Based on the generally accepted surface space charge layer model, the ethanol sensing process in the air can be summarized into the following three steps [42–44]:

(a) In fresh air: the oxygen molecules adsorb on the active sites (S_{active}) of the surface of the sensing materials and then dissociated into oxygen anion ions by trapping electrons from the conduction band (Eq. (1)), resulting in a depletion layer in the surface region and high resistance of the sensing materials. Meanwhile, it should be noted that the oxygen adsorption is a reversible process, namely, the adsorption and desorption of the oxygen take place simultaneously and the sensor resistance becomes stable once steady state is established.
(b) In the presence of ethanol: ethanol molecules react with the surface adsorbed oxygen ions following Eq. (2), which removes the oxygen and releases the trapped electrons back to the conduction band. As a result, the depletion layer is reduced, and the sensor resistance decreases. One important point is that oxygen from the air reoccupies the newly available active sites following Eq. (1) during the sensing reaction process. Obviously, this process is opposite to the ethanol reaction process and reduces the sensor response.
(c) Upon the removal of ethanol: oxygen from air re-adsorbs on the surface of the sensing materials following step (a), and the sensor resistance recovers to its initial state.

$$\frac{1}{2}O_2(ads) + ne^- + S_{active} \leftrightarrow O^{n-}(ads) \quad (1)$$

$$C_2H_5OH(gas) + O^{n-}(ads) \rightarrow P_r + S_{active} + e^{n-} \quad (2)$$

where the P_r is the reaction products and S_{active} is the active sites.

Eqs. (1), (2) indicate that oxygen molecules play an important bridge role in the ethanol sensing process. Thus, we compared the ethanol sensing behaviors in air and N_2 at 300 °C. As can be seen in Fig. 11, the first two sensing cycles were conducted with air as the background gas, resulting in a calculated response of 22.5, consistent with the results in Figs. 7 and 9. When the background gas is replaced by N_2, several interesting changes can be observed. First, the baseline resistance immediately drops significantly once the

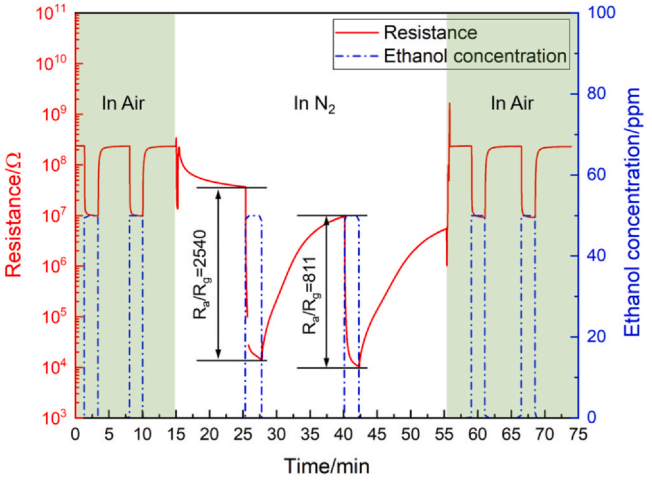

Fig. 11. Dynamic response and recovery curves of NiO/ZnO nanowires to 50 ppm ethanol at 300 °C with the background gases of air and N_2.

background is changed from the air to N_2. Next, the sensor shows a similarly fast response time upon exposure to ethanol in N_2 background to that in air. This suggests that the interaction process of ethanol and sensing material surfaces in air and N_2 is similar. Next, the ethanol response of the sensor in N_2 is much higher than that in the air. This seems contrary to the bridge role of oxygen in the ethanol sensing process that was discussed above. Finally, the recovery time in N_2 is much longer than that in air and the sensor does not recover to its initial state after more than 10 min in N_2, while the sensor fully recovers in less than 1 min in the air. Moreover, when the background gas is changed back to the air again, the baseline resistance and the sensing characteristics are fully recovered (see the fifth and sixth sensing cycles in Fig. 11).

Based on the above observation and discussion, a possible explanation of the different sensing behaviors in N_2 is proposed. When the sensor is in air, oxygen molecules adsorb on the active sites of the surface of the sensing material and then ionized to oxygen ions following Eq. (1). Based on previous reports, the oxygen vacancies (V^+) are one of the most important active sites [21,45]. When the background is changed to N_2, most of the adsorbed oxygen species are removed from the surface of the sensing materials, leading to a greatly reduced sensor resistance. When the ethanol is exposed to the sensor, different from the reaction in the air, the redox reaction may mainly take place between ethanol and surface lattice oxygen of the sensing material, which also releases the electrons, creating the surface vacancies, and consequently reducing the sensor resistance. Furthermore, because of the lack of oxygen, the created oxygen vacancies are hard to be healed. In other words, in N_2 background, only Eq. (2) takes place smoothly. This is hypothesized to be the main reason for the much higher ethanol response in N_2 than that in ethanol. Furthermore, although the high purity N_2 was used in this experiment, there may still be trace amount of oxygen in the gas delivery system. Therefore, as observed in Fig. 11, the sensor partially recovers with a very slow recovery rate. More efforts need to be done to reveal the complex gas sensing process reported here, which not only can help to understand the sensing mechanism but also plays an important role in designing the next generation gas sensors.

4. Conclusion

In summary, a two-step route was presented to synthesize NiO/ZnO heterostructured nanowires, which are composed of the host ZnO nanowires and NiO assembled on the outer surfaces. The diameters of the heterostructured nanowires are around 50 nm while their length can reach several micrometers. The gas sensing

properties were investigated by employing interdigitated Au electrodes on a miniature heater and using a computer-controlled dynamic gas sensing test platform. The optimum operating temperature of the sensor was determined to be 300 °C in consideration of both response magnitude and response/recovery times. At this operating temperature, the sensor exhibited a high response, and response and recovery times to ethanol. Furthermore, the sensor showed good reversibility, reproducibility, selectivity, stability, and robustness to humidity.

CRediT authorship contribution statement

Sikai Zhao: Conceptualization, Investigation, Writing - original Draft. **Yanbai Shen:** Conceptualization, Resources, Supervision, Writing - review & editing. **Roya Maboudian:** Conceptualization, Resources, Supervision, Writing - review & editing. **Yong Xia:** Writing - review & editing. **Aifei Pan:** Writing - review & editing. **Zhou Li:** Writing - review & editing. **Carlo Carraro:** Writing - review & editing..

Declaration of Competing Interest

The authors declare that they have no known competing financial interests or personal relationships that could have appeared to influence the work reported in this paper.

Acknowledgements

The project was supported by the National Natural Science Foundation of China (51674067, 51422402), Fundamental Research Funds for the Central Universities (N180102032, N180106002, N180408018), Liaoning Revitalization Talents Program (XLYC1807160), and Open Foundation of State Environmental Protection Key Laboratory of Mineral Metallurgical Resources Utilization and Pollution Control (HB201902). SZ, CC and RM acknowledge support of the U.S. National Science Foundation (grant # 1903188). SZ also acknowledges the support of China Scholarship Council (CSC). Special thanks are due to the instrument and data analysis from Analytica and Test Center, Northeastern University.

Appendix A. Supporting information

Supplementary data associated with this article can be found in the online version at doi:10.1016/j.jallcom.2021.160189.

References

[1] J. Zhang, X. Liu, G. Neri, N. Pinna, Nanostructured materials for room--temperature gas sensors, Adv. Mater. 28 (2016) 795–831.
[2] A. Tricoli, M. Righettoni, A. Teleki, Semiconductor gas sensors: dry synthesis and application, Angew. Chem. Int. Ed. 49 (2010) 7632–7659.
[3] X. Liu, S. Cheng, H. Liu, S. Hu, D. Zhang, H. Ning, A survey on gas sensing technology, Sensors 12 (2012) 9635–9665.
[4] S. Feng, F. Farha, Q. Li, Y. Wan, H. Ning, Review on smart gas sensing technology, Sensors 19 (2019) 3760.
[5] S. Zhao, Y. Shen, P. Zhou, X. Zhong, C. Han, Q. Zhao, D. Wei, Design of Au@WO_3 core–shell structured nanospheres for ppb-level NO_2 sensing, Sens. Actuators B Chem. 282 (2019) 917–926.
[6] R.A. Potyrailo, Multivariable sensors for ubiquitous monitoring of gases in the era of internet of things and industrial internet, Chem. Rev. 116 (2016) 11877–11923.
[7] S. Rackauskas, N. Barbero, C. Barolo, G. Viscardi, ZnO nanowire application in chemoresistive sensing: a review, Nanomater. (Basel, Switz.) 7 (2017) 381.
[8] E. De la Rosa, S. Sepúlveda-Guzman, B. Reeja-Jayan, A. Torres, P. Salas, N. Elizondo, M.J. Yacaman, Controlling the growth and luminescence properties of well-faceted ZnO nanorods, J. Phys. Chem. C. 111 (2007) 8489–8495.
[9] C. Daoyong, S. Jianian, Hydrothermal synthesis and gas sensing characters of ZnO nanorods, Sens. Actuators B Chem. 113 (2006) 526–531.
[10] F. Meng, Y. Chang, W. Qin, Z. Yuan, J. Zhao, J. Zhang, E. Han, S. Wang, M. Yang, Y. Shen, M. Ibrahim, ZnO-Reduced Graphene Oxide Composites Sensitized with Graphitic Carbon Nitride Nanosheets for Ethanol Sensing, ACS Appl. Nano Mater. 5 (2019) 2732–2742.
[11] X. Chen, Y. Shen, P. Zhou, X. Zhong, G. Li, C. Han, D. Wei, S. Li, Bimetallic Au/Pd nanoparticles decorated ZnO nanowires for NO_2 detection, Sens. Actuators B Chem. 289 (2019) 160–168.
[12] A.N. Afaah, Z. Khusaimi, M. Rusop, A review on zinc oxide nanostructures: doping and gas sensing, Advanced Materials Research, Trans. Tech. Publ. Ltd. Vol 667 (2013).
[13] C.M. Chang, M.H. Hon, I.C. Leu, Preparation of ZnO nanorod arrays with tailored defect-related characterisitcs and their effect on the ethanol gas sensing performance, Sens. Actuators B Chem. 151 (2010) 15–20.
[14] M.M. Arafat, B. Dinan, S.A. Akbar, A. Haseeb, Gas sensors based on one dimensional nanostructured metal-oxides: a review, Sensors 12 (2012) 7207–7258.
[15] S. Zhao, Y. Shen, P. Zhou, F. Hao, X. Xu, S. Gao, D. Wei, Y. Ao, Y. Shen, Enhanced NO_2 sensing performance of ZnO nanowires functionalized with ultra-fine In_2O_3 nanoparticles, Sens. Actuators B Chem. 308 (2020) 127729.
[16] P. Shankar, J.B.B. Rayappan, Monomer: design of ZnO nanostructures (Nanobush and nanowire) and their room-temperature ethanol vapor sensing signatures, ACS Appl. Mater. Interfaces 9 (2017) 38135–38145.
[17] N.J. Ridha, F.K.M. Alosfur, M.H.H. Jumali, S. Radiman, Dimensional effect of ZnO nanorods on gas-sensing performance, J. Phys. D Appl. Phys. 51 (2018) 435101.
[18] D.R. Miller, S.A. Akbar, P.A. Morris, Nanoscale metal oxide-based heterojunctions for gas sensing: a review, Sens. Actuators B Chem. 204 (2014) 250–272.
[19] C. Wang, X. Cheng, X. Zhou, P. Sun, N. Yamazoe, Hierarchical α-Fe_2O_3 /NiO composites with a hollow structure for a gas sensor, ACS Appl. Mater. Interfaces 15 (2014) 12031–12037.
[20] D. Zappa, V. Galstyan, N. Kaur, H.M.M.M. Arachchige, O. Sisman, E. Comini, "Metal oxide-based heterostructures for gas sensors"-a review, Anal. Chim. Acta 1039 (2018) 1–23.
[21] D. Degler, U. Weimar, N. Barsan, Current understanding of the fundamental mechanisms of doped and loaded semiconducting metal-oxide-based gas sensing materials, ACS Sens. 4 (2019) 2228–2249.
[22] J.M. Walker, S.A. Akbar, P.A. Morris, Synergistic effects in gas sensing semiconducting oxide nano-heterostructures: a review, Sens. Actuators B Chem. 286 (2019) 624–640.
[23] H.R. Kim, A. Haensch, I.D. Kim, N. Barsan, U. Weimar, J.H. Lee, The role of NiO doping in reducing the impact of humidity on the performance of SnO_2-Based gas sensors: synthesis strategies, and phenomenological and spectroscopic studies, Adv. Funct. Mater. 21 (2011) 4456–4463.
[24] S. Zhao, Y. Shen, P. Zhou, G. Li, F. Hao, C. Han, W. Liu, D. Wei, Construction of ZnO-SnO_2 n-n junction for dual-sensing of nitrogen dioxide and ethanol, Vacuum 181 (2020) 109615.
[25] H. Long, L. Chan, A. Harley-Trochimczyk, L.E. Luna, Z. Tang, T. Shi, A. Zettl, C. Carraro, M.A. Worsley, R. Maboudian, 3D MoS_2 aerogel for ultrasensitive NO_2 detection and its tunable sensing behavior, Adv. Mater. Interfaces 4 (2017) 1700217.
[26] A.C. Harley-Trochimczyk, Environmental gas sensing with high surface area nanomaterials on a low-power microfabricated heater platform, University of California, Berkeley, 2016.
[27] E. Comini, C. Baratto, G. Faglia, M. Ferroni, A. Vomiero, G. Sberveglieri, Quasi-one dimensional metal oxide semiconductors: Preparation, characterization and application as chemical sensors, Prog. Mater. Sci. 54 (2009) 1–67.
[28] S.Y. Bae, H.W. Seo, H.C. Choi, J. Park, J. Park, Heterostructures of ZnO nanorods with various one-dimensional nanostructures, J. Phys. Chem. B 108 (2004) 12318–12326.
[29] J. Xu, Z. Xue, N. Qin, Z. Cheng, Q. Xiang, The crystal facet-dependent gas sensing properties of ZnO nanosheets: experimental and computational study, Sens. Actuators B Chem. 242 (2017) 148–157.
[30] D. Zhang, Y. Jin, Y. Cao, Facile synthesis and ammonia gas sensing properties of NiO nanoparticles decorated MoS_2 nanosheets heterostructure, J. Mater. Sci. Mater. Electron. 30 (2019) 573–581.
[31] S. Zhao, Y. Shen, P. Zhou, J. Zhang, W. Zhang, X. Chen, D. Wei, P. Fang, Y. Shen, Highly selective NO_2 sensor based on p-type nanocrystalline NiO thin films prepared by sol–gel dip coating, Ceram. Int. 44 (2018) 753–759.
[32] S. Zhao, Y. Shen, X. Yan, P. Zhou, Y. Yin, R. Lu, C. Han, B. Cui, D. Wei, Complex-surfactant-assisted hydrothermal synthesis of one-dimensional ZnO nanorods for high-performance ethanol gas sensor, Sens. Actuators B Chem. 286 (2019) 501–511.
[33] X. Chen, Y. Shen, P. Zhou, S. Zhao, X. Zhong, T. Li, C. Han, D. Wei, D. Meng, NO_2 sensing properties of one-pot-synthesized ZnO nanowires with Pd functionalization, Sens. Actuators B Chem. 280 (2019) 151–161.
[34] U.K. Thakur, P. Kumar, S. Gusarov, A.E. Kobryn, S. Riddell, A. Goswami, K.M. Alam, S. Savela, P. Kar, T. Thundat, A. Meldrum, K. Shankar, Consistently high VOC values in pin type perovskite solar cells using Ni^{3+}-Doped NiO nanomesh as the hole transporting layer, ACS Appl. Mater. Interfaces 12 (2020) 11467–11478.
[35] W. Liu, C. Lu, X. Wang, K. Liang, B.K. Tay, In situ fabrication of three-dimensional, ultrathin graphite/carbon nanotube/NiO composite as binder-free electrode for high-performance energy storage, J. Mater. Chem. A 3 (2015) 624–633.
[36] Y. Shen, W. Wang, X. Chen, B. Zhang, D. Wei, S. Gao, B. Cui, Nitrogen dioxide sensing using tungsten oxide microspheres with hierarchical nanorod-assembled architectures by a complexing surfactant-mediated hydrothermal route, J. Mater. Chem. A 4 (2016) 1345–1352.
[37] Y. Shen, H. Bi, T. Li, X. Zhong, X. Chen, A. Fan, D. Wei, Low-temperature and highly enhanced NO_2 sensing performance of Au-functionalized WO_3 microspheres with a hierarchical nanostructure, Appl. Surf. Sci. 434 (2018) 922–931.
[38] H. Yuan, S.A.A.A. Aljneibi, J. Yuan, Y. Wang, H. Liu, J. Fang, C. Tang, X. Yan, H. Cai, Y. Gu, S.J. Pennycook, J. Tao, D. Zhao, ZnO nanosheets abundant in oxygen

vacancies derived from metal-organic frameworks for ppb-level gas sensing, Adv. Mater. (Deerfield Beach, Fla.) 31 (2019) 1807161.
[39] R. Xing, L. Xu, J. Song, C. Zhou, Q. Li, D. Liu, H. Wei Song, Preparation and gas sensing properties of In_2O_3/Au nanorods for detection of volatile organic compounds in exhaled breath, Sci. Rep. 5 (2015) 1–14.
[40] S. Zhao, Y. Shen, R. Maboudian, C. Carraro, C. Han, W. Liu, D. Wei, Facile synthesis of ZnO-SnO_2 hetero-structured nanowires for high-performance NO_2 sensing application, Sens. Actuators B Chem. 333 (2021) 129613.
[41] N. Illyaskutty, H. Kohler, T. Trautmann, M. Schwotzer, V.P.M. Pillai, Enhanced ethanol sensing response from nanostructured MoO_3:ZnO thin films and their mechanism of sensing, J. Mater. Chem. C 1 (2013) 3976–3984.
[42] W. Zhang, Y. Fan, T. Yuan, B. Lu, Y. Liu, Z. Li, G. Li, Z. Cheng, J. Xu, Ultrafine tungsten oxide nanowires: synthesis and highly selective acetone sensing and mechanism analysis, ACS Appl. Mater. Interfaces 12 (2020) 3755–3763.
[43] N. Barsan, D. Koziej, U. Weimar, Metal oxide-based gas sensor research: how to? Sens. Actuators B Chem. 121 (2007) 18–35.
[44] Shen Yanbai, Wang Wei, Fan Anfeng, et al., Highly sensitive hydrogen sensors based on SnO_2 nanomaterials with different morphologies, Int. J. Hydrog. Energy (2015).
[45] Z. Wang, J. Xue, D. Han, F. Gu, Controllable defect redistribution of ZnO nanopyramids with exposed {1011} facets for enhanced gas sensing performance, ACS Appl. Mater. Interfaces 7 (2015) 308–317.